processes

MDPI

Article

A Database Extension for a Safety Evaluation of a Hydrogen Refueling Station with a Barrier Using a CFD Analysis and a Machine Learning Method

Hyung-Seok Kang [1,*], Ji-Won Hwang [2] and Chul-Hee Yu [3]

[1] Korea Atomic Energy Research Institute, Daejeon 34057, Republic of Korea
[2] Dahan Tech Inc., Seoul 06106, Republic of Korea; wonny@dahan.co.kr
[3] Korea Gas Safety Corporation, Yeongwol-gun 26203, Republic of Korea; gusari@kgs.or.kr
* Correspondence: hskang3@kaeri.re.kr; Tel.: +82-42-868-8948

Abstract: A methodology is proposed to extend datasets in a database suitable for use as a reference tool to support an evaluation of damage mitigation by a barrier wall in a hydrogen refueling station (HRS) during a vapor cloud explosion (VCE) accident. This is realized with a computational fluid dynamic (CFD) analysis and machine learning (ML) technology because measured data from hydrogen explosion tests with various installed barrier models usually require considerable amounts of time, a secured space, and precise measurements. A CFD sensitivity calculation was conducted using the radXiFoam v1.0 code and the established analysis methodology with an error range of approximately ±30% while changing the barrier height from that was used in an experiment conducted by the Stanford Research Institute (SRI) to investigate the effect of the barrier height on the reduction in peak overpressures from an explosion site to far fields in an open space. The radXiFoam code was developed based on the open-source CFD software OpenFOAM-v2112 to simulate a VCE accident in a humid air environment at a compressed gaseous or liquefied HRS. We attempted to extend the number of datasets in the VCE database through the use of the ML method on the basis of pressure data predicted by a CFD sensitivity calculation, also uncovering the possibility of utilizing the ML method to extend the VCE database. The data produced by the CFD sensitivity calculation and the ML method will be examined to confirm their validity and applicability to hypothetical VCE accident simulations if the related test data can be produced during experimental research. The database constructed using core data from the experiment and extended data from the CFD analysis and the ML method will be used to increase the credibility of radXiFoam analysis results for VCE accident scenarios at HRSs, ultimately contributing to safety assurances of HRSs in Republic of Korea.

Keywords: hydrogen energy; hydrogen refueling station; barrier; vapor cloud explosion; peak overpressure; CFD; OpenFOAM; machine learning; safety evaluation

Citation: Kang, H.-S.; Hwang, J.-W.; Yu, C.-H. A Database Extension for a Safety Evaluation of a Hydrogen Refueling Station with a Barrier Using a CFD Analysis and a Machine Learning Method. *Processes* **2023**, *11*, 3025. https://doi.org/10.3390/pr11103025

Academic Editors: Omar Dario Lopez Mejia and Santiago Lain

Received: 29 September 2023
Revised: 13 October 2023
Accepted: 14 October 2023
Published: 20 October 2023

1. Introduction

To build a stronger economic society using hydrogen energy in Republic of Korea, a roadmap for the construction of 1200 hydrogen refueling stations (HRSs) for transportation vehicles by 2040 was proposed by the Korean government [1,2]. However, this plan is facing delays when compared to the original timeline, as residents around the HRS sites to be built in a large city are opposing its construction. They claim that HRSs are not safe, referring to an explosion accident that occurred at a compressed hydrogen storage tank connected to a water electrolysis facility in Gangwon technopark in Republic of Korea [3]. In addition, the memory of a hydrogen explosion accident at a nuclear power plant in Japan and its detrimental effects on the environment continually enhances residents' anxiety over the use of hydrogen energy in Republic of Korea [4–6]. From the end of 2023, liquefied hydrogen (LH2) will be produced in large quantities at several facilities and supplied to consumers through LH2 hydrogen stations in Republic of Korea [7]. Thus, the residents' concerns

over the safety of HRSs are considerably greater because stations with LH2 contain more hydrogen compared to typical refueling stations.

The Korea Gas Safety Corporation (KGS), the organization responsible for the safety of hydrogen energy facilities in Republic of Korea, decided to reinforce the specific technical regulations pertaining to HRSs to increase safety on the basis of experimental research and numerical simulations [8]. One such effort is specifically to present a method by which to devise a standard model for a damage-mitigation wall, also referred to as a barrier, around the storage tanks at a HRS or the boundary of a HRS on the basis of the results of a quantitative risk assessment (QRA) and based on the distance between the storage tank at the HRS and the facilities surrounding the HRS [8–10]. To perform the QRA, various accident scenarios should be taken into account after investigating the possibility of a hydrogen gas release from certain components and the corresponding frequencies based on datasets and the design of the HRS [11]. The extent of such damage resulting from each accident scenario, including individual risk and social risk levels, must be predicted using a verified computational code [12].

The most frequent and damaging type of accident in resident areas around a HRS, transferring the damaging effects over long distances from the explosion site considering various accident scenarios, may be a vapor cloud explosion (VCE), which occurs due to hydrogen released from a storage tank into an air environment at a HRS [13]. This likely stems from how the pressure wave propagates at the speed of sound to distant locations in all directions in an air environment from the explosion site at the HRS as soon as the pressure builds due to the combustion energy released from the hydrogen–air chemical reaction. If a pressure wave with a magnitude exceeding a certain value, as shown in Table 1, arrives at structures or where people are, harmful effects, such as broken glass or even ear injuries, may occur [14,15]. Thus, a three-dimensional computational fluid dynamic (CFD) code is useful for quantitatively evaluating the propagation of pressure waves due to a VCE at an HRS because pressure waves generally tend to lose strength as well as change direction when colliding with structures around an HRS as they propagate through air [16]. In addition, applying the CFD codes, including the open-source software OpenFOAM, for a VCE analysis has been conducted wildly in the areas of process safety and loss prevention [17].

Table 1. Damage criteria according to overpressure values [14,15].

Overpressure (kPa)	Damage Effect
0.2	Partially broken windows
1	Breaking glass
3	Minor damage to structures and injuries to people
5	Broken structures in houses
7	Partially damaged houses and much harm to people
14	Starting value for lethal effects on humans
15	Slightly damage to roofs and walls of structure
18	Approximately 50% of houses damaged per block
20	Steel structure of building is damaged and pulling away from the foundation
35–50	Structure destroyed

We developed a CFD code, radXiFoam, using OpenFOAM-v2112 to simulate a VCE accident in a humid air environment at an HRS after validation through several test results, which included the overpressure reduction effect by a barrier [18,19]. We used open-source software because we can freely distribute radXiFoam to engineers who work on the safety of HRSs. The released radXiFoam will be used to predict harmful effects due to hypothetical VCE accidents at HRSs, and the QRA, on the basis of the predicted CFD results, will be reviewed by the KGS to approve the safety evaluation results for HRSs before the granting of a construction permit from the licensing institute.

To increase the confidence of hypothetical VCE accident analysis results, using radXiFoam as a reference tool, we used a database consisting of experimental data and validated analysis data fed into radXiFoam with an error range to utilize quantitative data to describe the barrier effect of overpressure reduction on several VCE types. Herein, radXiFoam analysis results validated against test data can provide overpressure data at various locations where measurement devices are not installed, as well as visualized pressure contours from the explosion site to a far-field in an air environment. The datasets in the database can provide criteria to safety engineers, who must judge the credibility of radXiFoam results before using the calculated overpressures through the barrier as the QRA inputs, as the CFD results for hydrogen explosions occurring around structures in open spaces tend to vary according to the geometrical model, the mesh distribution in the grid model, the numerical and empirical constants used in the CFD models, and the time step size in the transient calculation [20]. Such efforts to use databases for safety evaluations of gas explosion accidents are also underway in other countries [21–23].

However, it is difficult to obtain sufficient VCE test data with various barrier models in a short period before starting to construct HRSs actively around protected facilities because gas explosion tests usually require safe experimentation at secured locations [24,25]. One feasible means of overcoming this difficulty in obtaining the data is to extend the database using CFD sensitivity calculations on the basis of validated radXiFoam results for VCE test data with the installation of the barrier. In addition, we are now considering the use of a machine learning (ML) method [26] to produce new datasets based on existing data in the VCE database when no available data for a certain HRS exists in the database. However, this idea of using the ML method to generate datasets for a safety evaluation should be examined if the related data can be produced in our experimental research [8], despite the fact that this type of trial using the ML method to reinforce a database is currently used in other industries [27].

2. Use of the VCE Database for HRS' Safety Evaluations

To build a database to be used as a reference tool for a hypothetical VCE scenario analysis at an HRS with a barrier, first we collected published test data produced by a foreign institute, in this case, Stanford Research Institute (SRI) [24,25,28]. The plan is to add Republic of Korea's own hydrogen explosion test results by installing various barrier models to the VCE database after analyzing the data, with this enacted by the KGS and other institutes [8]. According to the test plan, a hydrogen–air mixture volume of 40 m^3 with the barrier installed will be exploded to measure the overpressure reduction through the barrier. This may create unique data which can extend the range of the database because previous VCE tests with the installation of such a barrier were generally gained when using a hydrogen–air mixture volume of 5.2 m^3 under a stoichiometric condition [24,25,28]. The datasets of the overpressure in the VCE database will be categorized according to the hydrogen–air mixture volume, hydrogen concentration, ignition method, existence of obstacle geometries, weather conditions, and the barrier model. Such a categorized database will contain the criteria to be used to anticipate the hydrogen explosion strength, the harmful effects, and the degree of damage mitigation by the barrier.

Safety engineers can compare their VCE accident analysis results, which will be used as the input for the QRA, with the suitable datasets in the database if conditions similar to those of the accident scenarios, such as the hydrogen concentration, relative humidity of the air, and the distributed range of the hydrogen–air mixture, exist in the database, as shown in Figure 1. This comparison can increase the credibility of the VCE accident analysis results by radXiFoam because CFD results basically have uncertainty arising from the modeling process of the VCE accident scenarios [20]. Thus, the database should contain a broad range of data related to VCE accident scenarios at HRSs, including several barrier models, to the greatest extent possible, to increase the credibility of safety evaluations of HRSs to be constructed with a barrier around protected facilities so as to meet KGS regulations. Therefore, the data produced by radXiFoam sensitivity calculations for various

barrier models can be efficiently used to increase the utilization of the VCE database, as such data compensate for the lack of test data stemming from the limited gas explosion experiments. If the ML can properly produce reference data for HRSs, which will be constructed in various areas in large cities, using a published theory based on existing datasets in a database [26,29], safety engineers can use the produced data as reference materials for comparisons with calculated radXiFoam results for a VCE accident analysis.

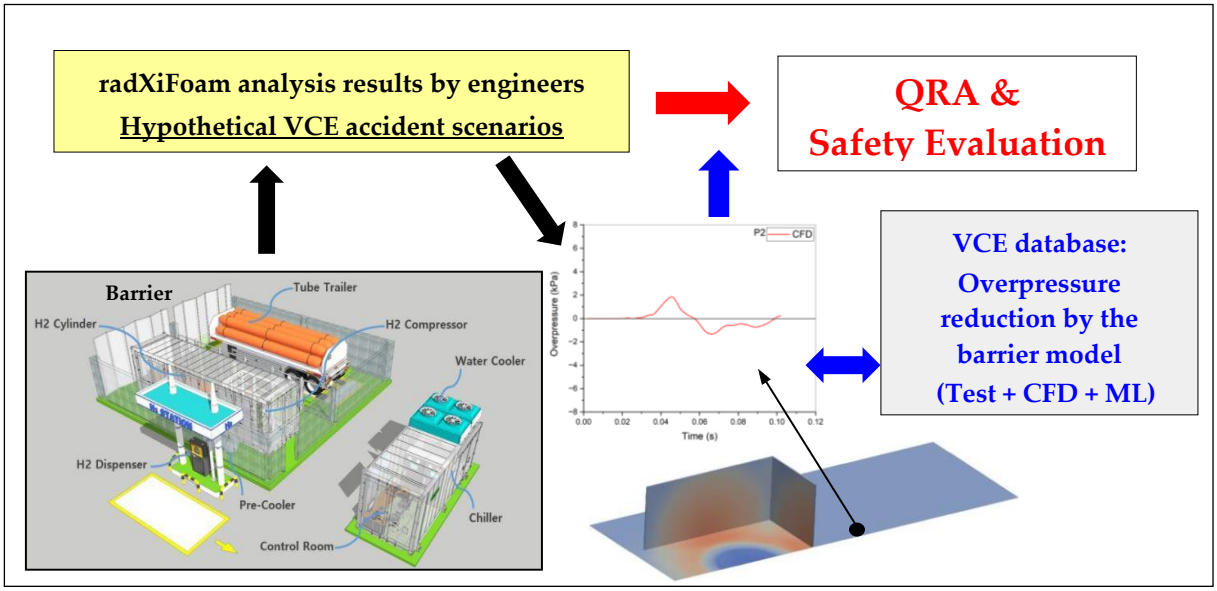

Figure 1. Plan for the utilization of the VCE database.

3. Producing Datasets Using the CFD Analysis

3.1. RadXiFoam Solver

We developed an open-source CFD solver, radXiFoam, to simulate a VCE accident in a humid air environment at a HRS and its damaging effects on residents around a HRS on the basis of XiFoam implemented in OpenFOAM-v2112 [18,19]. The combustion solver XiFoam, using a flamelet progress variable model, is usually applied to simulate the flame acceleration phenomena in a premixed combustion area considering an effective computational cost when compared to a solver based on a detailed chemical kinetic model [30]. However, XiFoam does not currently simulate humid air conditions, which may affect the VCE analysis results, as XiFoam only considers the transport equations of species for the fuel mixture fraction (ft) and regress variable (b) [19]. From the calculated results of ft and b in the fuel-oxygen mixture, XiFoam can calculate only the mass fraction of the fresh fuel and the burnt fuel in an inhomogeneous mixture model in OpenFOAM-v2112.

Therefore, we added species equations for the water vapor (wv) and nitrogen gas (n_2) to the existing species equation in XiFoam (Equation (1)) to consider a humid air condition, setting the relative humidity to 40%, and developed what is termed the vaporInnhomogeneous mixture model, which can calculate the variations in the gas concentrations in a hydrogen–air mixture as the combustion proceeds [18]. In Equation (1), the variable i indicates a certain species, such as water vapor or nitrogen gas. In addition, we implemented a radiative heat transfer term to the energy equation into XiFoam (Equation (2)) to calculate the precise enthalpy variation in the mixture of hydrogen, air, and water vapor, as the existence of water vapor may affect the heat transfer phenomenon through the absorption and emittance of thermal photons discharged from the combustion region.

To simulate thermal photon absorption by water vapor accurately according to the relevant concentration in the air, we modified "GreyMeanAbsorptionEmission.H" in XiFoam to include the partial pressure of the water vapor (p_{wv}) in the gas mixture to calculate the absorption coefficient (a_{wv}) and then proposed it as "VaporGreyMeanAbsorptionEmission.H" in radXiFoam. In Equation (3), k_{wv} is the absorption coefficient depending on the

gas temperature [31]. For a radiative heat transfer model, first we apply the P-1 radiation model (Equation (4)) to calculate the radiative heat transfer through the water vapor in the air, which is described in detail in the literature [32,33]. We also proposed an effective correlation model (Equation (5)) for the laminar flame speed based on the fuel equivalent ratio in the hydrogen–air mixture considering the initial water vapor, which was modified from a complicated form implemented in XiFoam [18,33–35]. In Equation (5), T_u is the unburnt gas temperature, T_o is the reference temperature (300 K), p is the pressure, p_o is the reference pressure (1 bar), S_{uo} is the laminar flame speed in the reference condition, and φ is the fuel equivalence ratio.

$$\frac{\partial(\rho Y_i)}{\partial t} + \nabla\cdot(\rho U Y_i) - \nabla\cdot\left[\left(\frac{\mu_t}{Sc_t}\right)\nabla Y_i\right] = S_i \tag{1}$$

$$\frac{\partial}{\partial t}(\rho h) + \nabla\cdot(\rho U h) + \frac{\partial}{\partial t}(\rho K) + \nabla\cdot(\rho U K) - \frac{\partial p}{\partial t} + \nabla\cdot\left(\frac{\mu_t}{Sc_t}\nabla h\right) = -\nabla\cdot q_r \tag{2}$$

$$a_{wv} = k_{wv} \times p_{wv} \tag{3}$$

$$\nabla\cdot q_r = aG - 4\left(e\sigma_{SB}T^4 + E\right) \tag{4}$$

$$S_u = S_{uo}\left(\frac{T_u}{T_o}\right)^{\alpha}\left(\frac{p}{p_o}\right)^{\beta} \tag{5}$$

$$\alpha = 2.18 - 0.8(\varphi - 1) \tag{6}$$

$$\beta = -0.16 + 0.22(\varphi - 1) \tag{7}$$

3.2. Analysis of SRI Test 4-02 Using radXiFoam

In order to determine whether radXiFoam can accurately simulate the VCE phenomena and the overpressure decrease due to the use of a barrier in an air environment, a validation analysis was conducted on the basis of measured data from SRI Test 4-02 [24,25]. SRI conducted a gas explosion test using a hydrogen–air mixture volume of 5.2 m^3 under a stoichiometric condition of approximately 30 vol.% with the installation of a barrier, as shown in Figure 2 and Table 2 [24,25]. The barrier, which had a height of 2 m, width of 10 m, and thickness of 0.1 m, was located 5.1 m from the ignition point in a tent to reduce the propagation of the damaging effects due to the VCE. The gas explosion in the tent was started using an electric spark device, which emitted a spark for 2 ms, located 2.5 cm above the center of the bottom plate, with the removal of the plastic film that covered the boundary of the tent. An obstacle type of geometry to induce flame acceleration was not used, except for the supporting bars of the plastic film and the measurement devices in the tent. Pressure sensors to measure the overpressure reduction due to the barrier were located 2 m behind (P2) and 2 m in front (P4) of the barrier, as shown in Figure 2, also measuring the overpressure increase owing to the VCE in the tent (P3). The overpressures at 11 m, 21 m, and 41 m from the ignition point were also measured to record the characteristics of the pressure wave propagation behind the barrier.

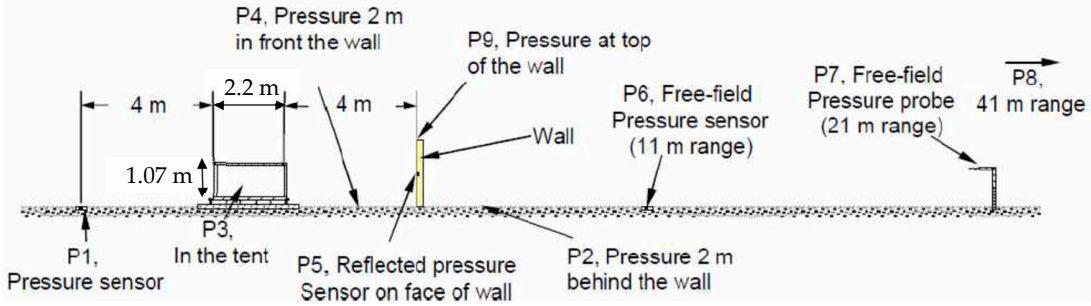

Figure 2. Schematic diagram of the SRI test facility [24].

Table 2. Conditions of the SRI hydrogen explosion tests [24,25].

Test No.	H_2–Air Mixture Volume (m^3)	H_2 Con. (vol.%)	Ambient Temp. (K)	Wind (m/s)	Ignition Method	Barrier Existence
4-02	5.2	29.9	283.45	2.0	Electric spark	O

Barrier dimensions: Height × Width × Thickness = 2 m × 10 m × 0.1 m.

A three-dimensional grid model utilizing a half-symmetric condition to simulate the SRI test facility was developed using the blockMesh utility in OpenFOAM-v2112 [19], as shown in Figure 3. To determine the horizontal length along the x-direction in the grid model, we considered a required separation distance of 30 m between the HRS and the first protected facilities located around the HRS in the KGS codes [9,10]. Thus, we did not include pressure sensor P8, located 41 m from the ignition point in the grid model, to reduce the computational time. We also decreased the width of the grid model to 5 m from the distance of 10 m used in a previous analysis [36] to ensure effective sensitivity calculations of the various barrier heights during a suitable computational time. A total of 2,569,440 hexahedral cells with an approximate cell length of 1.5 cm around the tent region and 15 to 25 cm at the far field region from the tent were generated in the grid model to resolve the rapid flame acceleration due to the spark ignition and the propagation of the pressure wave in the air environment. The cell length sizes in the grid model were determined based on previous mesh sensitivity calculation results [36]. The boundary conditions for the grid model are shown in Figure 3a. The opening condition allows for the inflow and outflow of air through the applied surfaces and simultaneously uses a wave transmissive outflow condition that can be expressed by Equations (8) and (9) [19,36]. In Equation (9), W_p is the patch wave speed, ϕ_p is the patch face flux, S_f is the patch face area vector, φ_p is the patch compressibility, and γ is the ratio of specific heat. A patch refers to a surface on which the opening condition is applied. An emissivity value of 0.072 was assigned to the bottom wall region in the tent on the basis of radiative property literature [32] on the simulation of the radiative heat transfer from a combusted gas to a steel wall.

$$\left.\frac{DW_p}{Dt}\right|_{outflow} = 0 \tag{8}$$

$$W_p = \frac{\varnothing_p}{|S_f|} + \sqrt{\frac{\gamma}{\varphi_p}} \tag{9}$$

The initial conditions used to simulate the test conditions in Table 2, including the hydrogen concentration in the tent, were given as the corresponding hydrogen mass fraction (ft), as shown in Figure 3b, using the utility program setFields in OpenFOAM-v2112 [18,19]. The spark ignition model, previously developed on the basis of other SRI test cases [24,25], used to initiate the hydrogen combustion in the tent region, was applied to simulate electric spark operation for 2 ms with an equivalent energy of 40 J [20]. To capture the pressure wave propagation and reflection accurately after collision with the barrier in the air environment, we used a small time step of approximately 1.0×10^{-6} s to 1.0×10^{-4} s in the transient calculation time of 0.1 s.

The calculated temperature and pressure distribution on the symmetric plane using radXiFoam with the established methodology (Table 3) over time are correspondingly shown in Figures 4 and 5, which indicate that the results reasonably predict the progress of the VCE from the ignition in the tent region to the pressure wave propagation to the air environment with the formation of a semi-spherical pressure band. The pressure buildup in the combustion region results from the combustion energy due to the hydrogen–air chemical reaction, which progresses continually as the flame propagates in the tent region. Figure 5 shows that the barrier effectively prevents pressure wave propagation along the horizontal x-direction, i.e., from the tent region to the air environment. As a result of this prevention, the pressure in the region below the barrier height is lower than those of other

regions in the rear area of the barrier. Thus, the calculated peak overpressure of 5.27 kPa at P4, located 2 m in front of the barrier, is reduced to 1.67 kPa at P2 at 2 m behind the barrier. The comparison of pressure waves at the local positions of P2, P4, P6, and P7 shows that the CFD results accurately predict the measured peak overpressures with an error range of approximately ±30%, as shown in Figure 6. However, the predicted pressure waves at each measurement location pass approximately 28 ms faster than in the test data. This can be explained by the fact that we neglected the transition period from the laminar flame to the turbulent flame by assuming fully turbulent mixing and combustion in the spark ignition model.

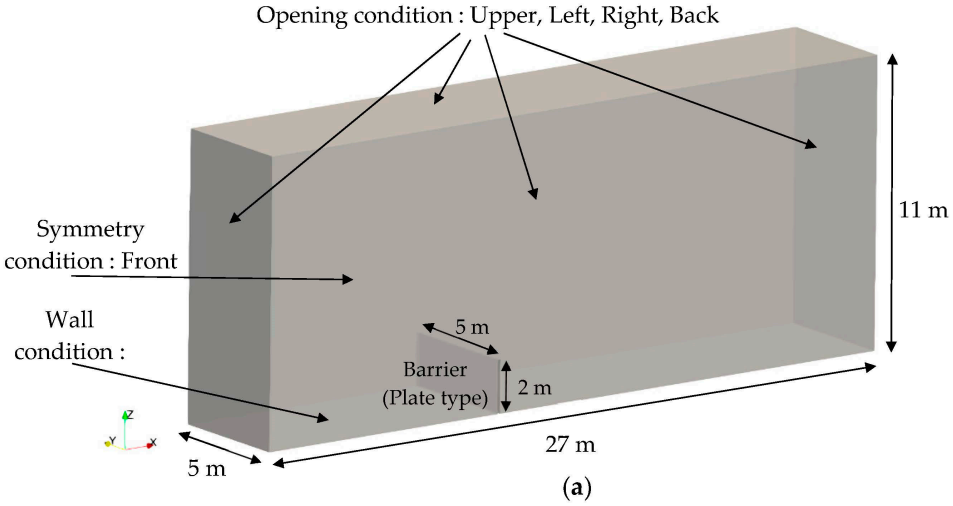

(**a**)

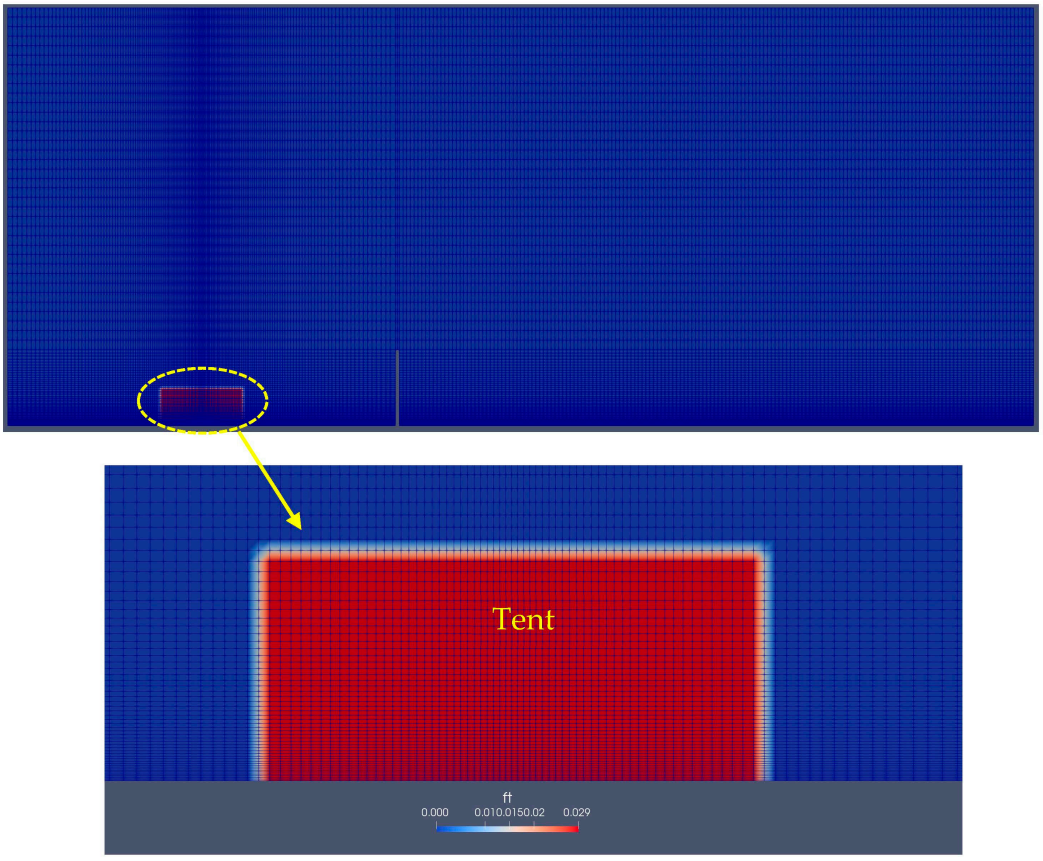

(**b**)

Figure 3. Grid model of the SRI Test 4-02 facility: (**a**) Geometric model and boundary conditions; (**b**) Mesh distribution and hydrogen mass fraction (ft) in the grid model.

Table 3. Analysis methodology for the VCE explosion test with a barrier.

Parameter	Models
• Open-source software	radXiFoam v1.0 based on OpenFOAM-v2112
• Thermal–hydraulic solver algorithm	PIMPLE [19]
• Combustion model	Flamelet progress variable
• Turbulence model	k-ω SST
• Wall function	kqR/omega
• CFL number	<0.8
• Mesh type	Hexahedral
• Mesh size at the far field	~25 cm
• Ignition model	Spark ignition model

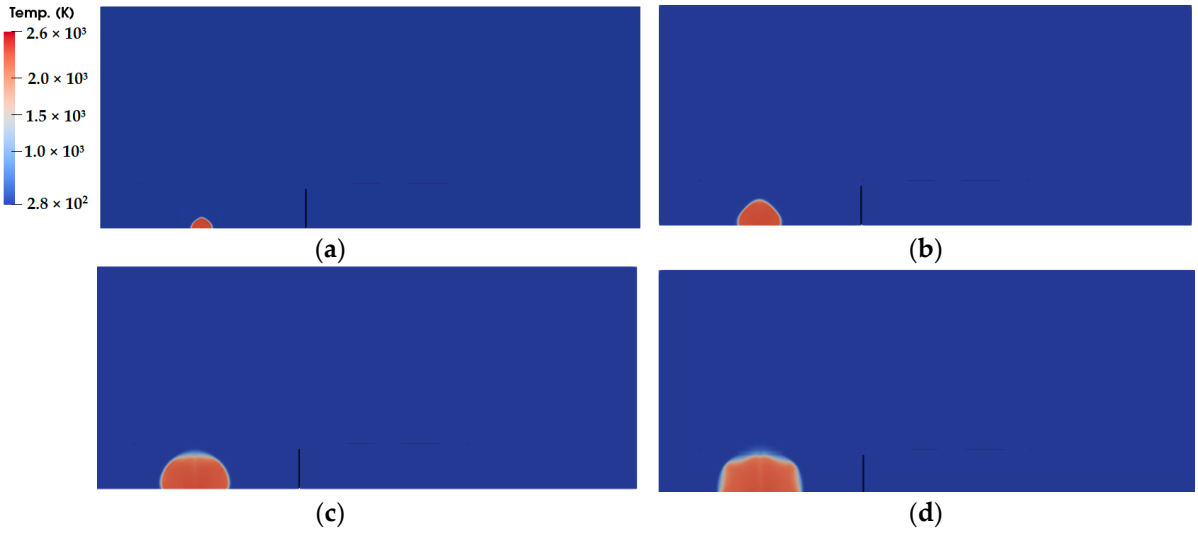

Figure 4. Temperature distribution over time (front view): (**a**) t = 0.01 s; (**b**) t = 0.02 s; (**c**) t = 0.03 s; (**d**) t = 0.04 s.

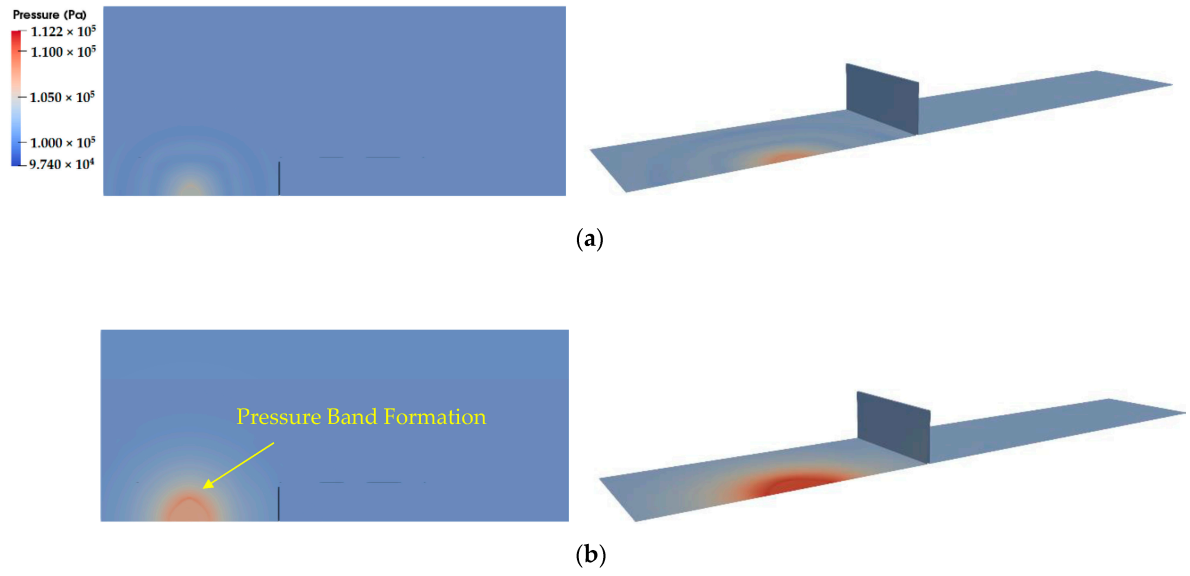

Figure 5. *Cont.*

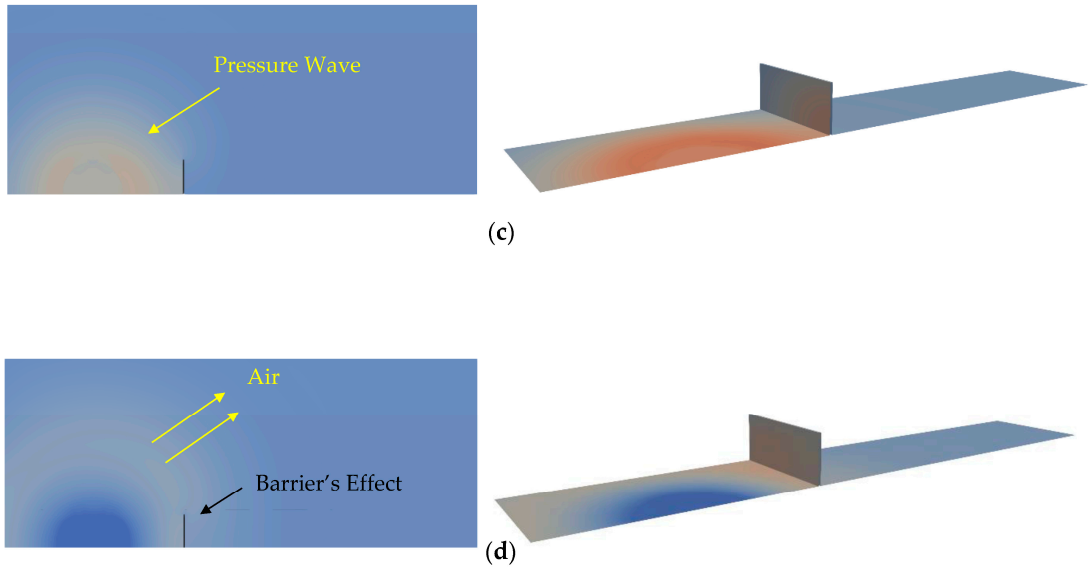

Figure 5. Pressure distribution on symmetry and wall planes: (**a**) t = 0.01 s; (**b**) t = 0.02 s; (**c**) t = 0.03 s; (**d**) t = 0.04 s.

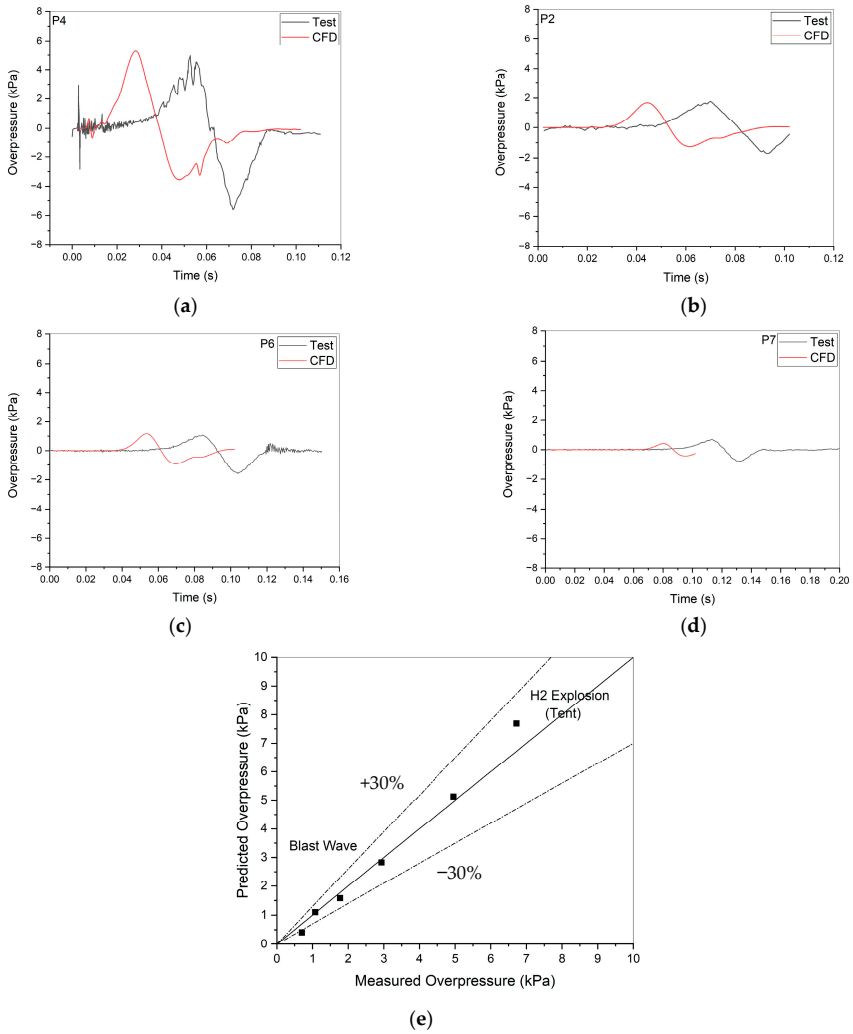

Figure 6. Comparison of overpressures at local positions between the test data and the CFD results: (**a**) P4 (2 m front of the barrier); (**b**) P2 (2 m behind the barrier); (**c**) P6 (range: 11 m); (**d**) P7 (range: 21 m); (**e**) Prediction uncertainty.

3.3. CFD Sensitivity Calculation Results and Discussion

To assess the effect of the barrier height on the reduction in the overpressure due to the VCE, we conducted a sensitivity calculation while changing only the barrier height from 2 m to 3 m and 4 m in the input files and with the established analysis methodology used for the SRI Test 4-02 calculation (Table 4), as we judged that the height variation in the barrier had an obvious effect on the overpressure reduction on the basis of simulation results from an overseas institute [28]. We carefully controlled the input parameters for the blockMesh utility to produce a nearly identical mesh distribution around the barrier between the grid models for Cases−1 to −4 to eliminate the mesh dependency on the calculated pressure distribution. In addition, we calculated Case−1 again using a new grid model, in which the width only extended from 5 m to 10 m, to investigate the effect of the location of the outflow condition along the *y*-direction in the grid model on the pressure field calculation (Case−4). It is expected that the comparison results of the local overpressures between Case−1 and Case−4 will produce a good guideline for the development of a grid model to analyze hypothetical VCE accident scenarios at HRSs to be performed by safety engineers.

Table 4. Sensitivity calculation on the basis of a CFD simulation for SRI Test 4-02.

Case No.	Barrier Height (m)/Width (m)/R (m)	Grid Model Length (m)/Width (m)/Height (m)	Number of Cells (Grid Model)
Case−1	2/0.1/5.1	27/5/11	2,569,440
Case−2	3/0.1/5.1	27/5/11	2,568,800
Case−3	4/0.1/5.1	27/5/11	2,568,160
Case−4	2/0.1/5.1	27/10/11	3,478,390

Range (m): horizontal distance from the ignition point.

The CFD sensitivity calculation results for various barrier heights of 2 m, 3 m, and 4 m (Figure 7a–c) show that the height of the pressure wave that propagates from the tent region to the air environment blocked by the barrier is increased as the barrier height increases. This feature indicates that the affected area on the ground in the rear region of the barrier from the propagating pressure wave is also increased as the barrier height increases. As a result of these effects according to the barrier height, the predicted peak overpressures at the P2 location are decreased from approximately 1.7 kPa to 0.85 kPa as the barrier height is increased from 2 m to 4 m (Figure 8a). This distinct difference may stem from the fact that the magnitude of the pressure wave and the elevation of the pressure band formation around the tent region are nearly identical regardless of the barrier height because the exploded hydrogen–air volume in the tent region is equal to 5.2 m^3 in Cases−1 to 3.

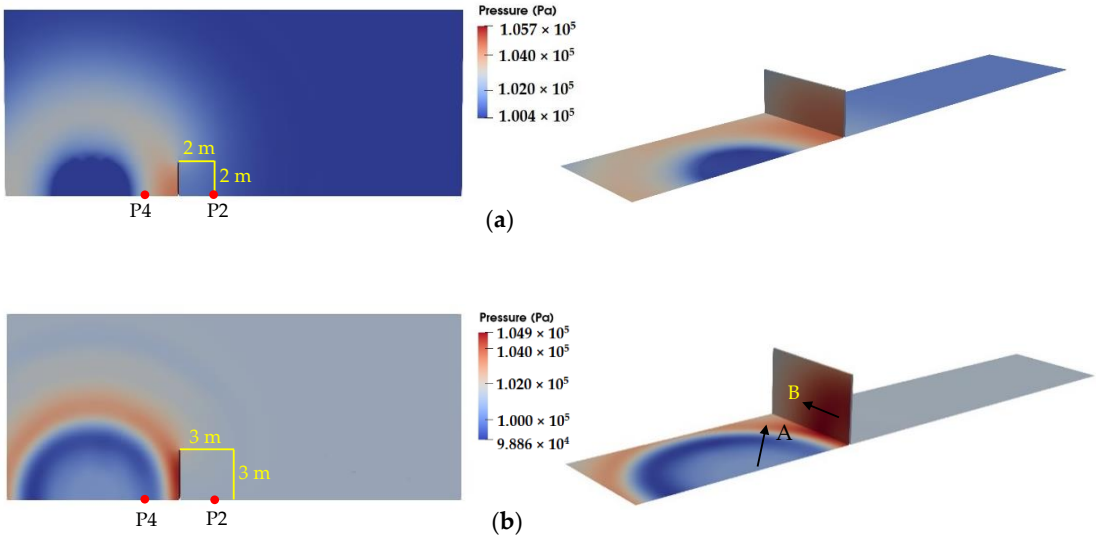

Figure 7. *Cont.*

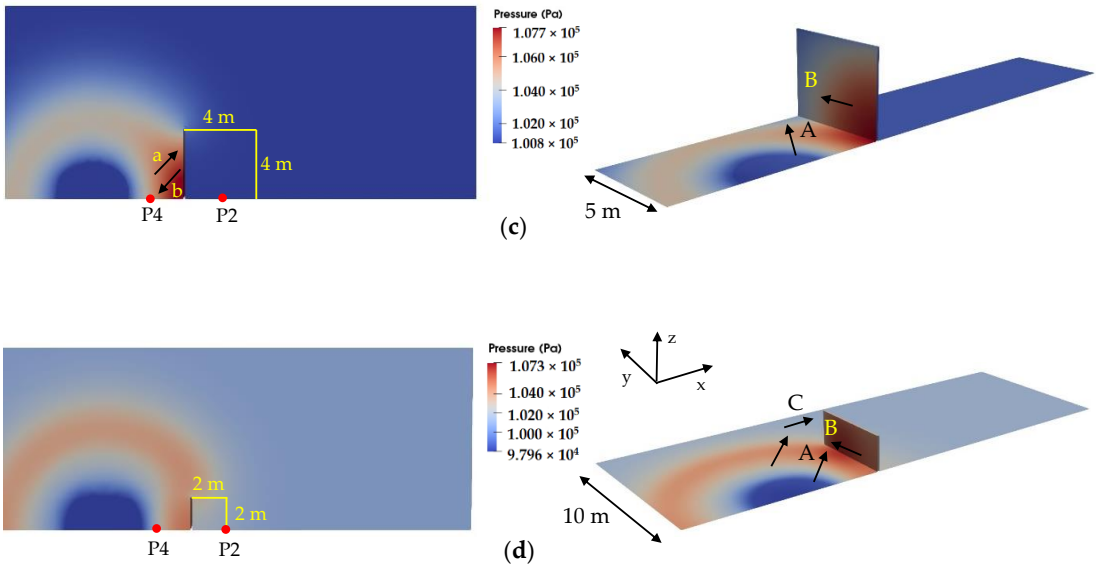

Figure 7. Pressure distribution on symmetry and wall planes according to the case: (**a**) t = 0.037 s (Case−1); (**b**) t = 0.030 s (Case−2); (**c**) t = 0.031 s (Case−3); (**d**) t = 0.034 s (Case−4); A (Pressure wave propagating to the outer region from the tent region); B (Reflected pressure wave propagating to the outer region along the surface of the barrier); C (Pressure wave propagating to the outer region after bypassing the barrier); a (Pressure wave propagating to the barrier from the ten tent region); b (Reflected pressure wave propagating to the location of P4 from the barrier).

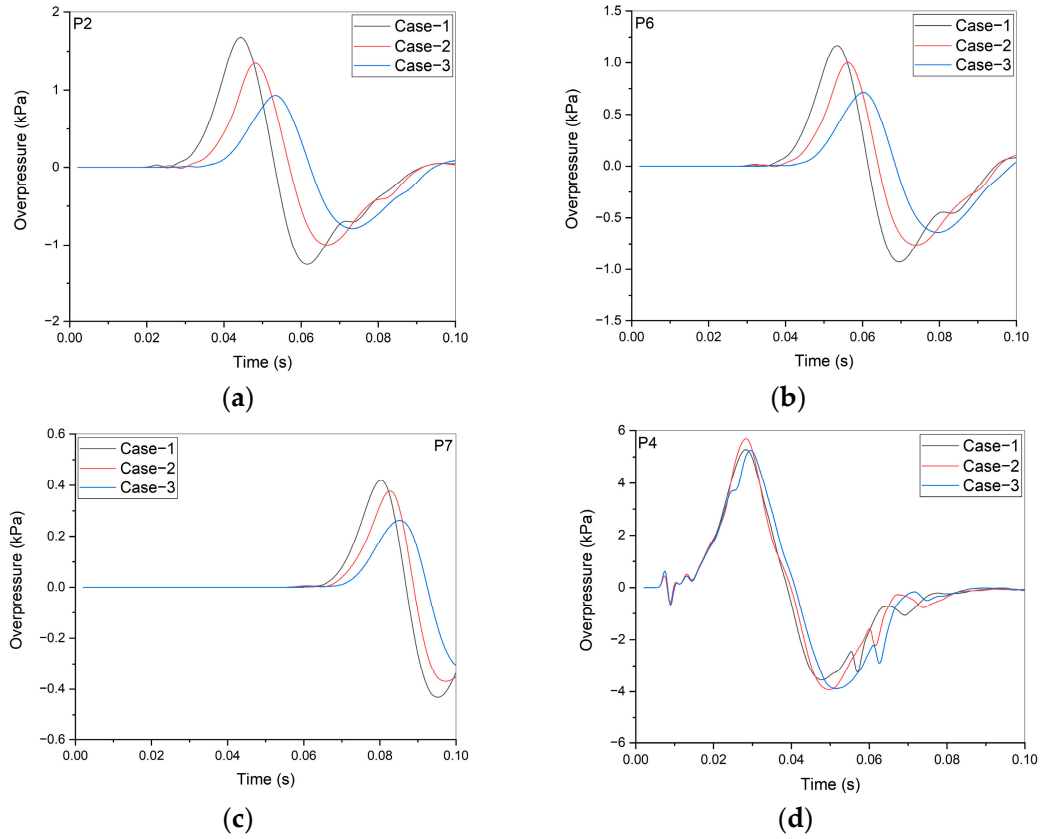

Figure 8. Comparison of overpressures at local positions between Cases−1, 2 and −3: (**a**) P2 (2 m behind the barrier); (**b**) P6 (range: 11 m); (**c**) P7 (range: 21 m); (**d**) P4 (2 m front of the barrier).

However, the calculated overpressures at P4, of which the location is 2 m in front of the barrier, show no significant differences between the cases tested here, as shown in Figure 8d. This result can be explained by the fact that the propagation of the pressure wave in front of

the barrier proceeds continually as hydrogen combustion takes place from the tent region to the outward region along the y-direction while maintaining a hemi-spherical-type shape on the ground (Figure 7b–d, "A"). The reflected pressure wave after the collision with the barrier (Figure 7b–d, "B") mainly flows to the outward region along the y-direction on the surface of the barrier because the strength of the pressure wave from the tent region exceeds that of the pressure wave reflected from the barrier.

As a result of this propagation pattern of the pressure wave in front of the barrier, the location of the wave transmissive outflow condition, for which the Neumann condition for the wave velocity applies (Equation (8)), may affect the calculation of the pressure field in the area in front of the barrier by radXiFoam using the PIMPLE algorithm (Figure 9a) [19]. In addition, this effect appears to exist in the calculated overpressure at the P2 location in the rear region of the barrier (Figure 9b). This can be explained by the fact that the direction of the pressure wave passing the barrier along the y-direction turns to the P2 location despite the fact that the corresponding wave's strength is considerably decreased. Therefore, we can conclude that the wave outflow condition in the VCE simulation should be located at some distance away from the explosion site to calculate the pressure field accurately when assuming proper pressure wave decay while the wave propagates to the outflow region.

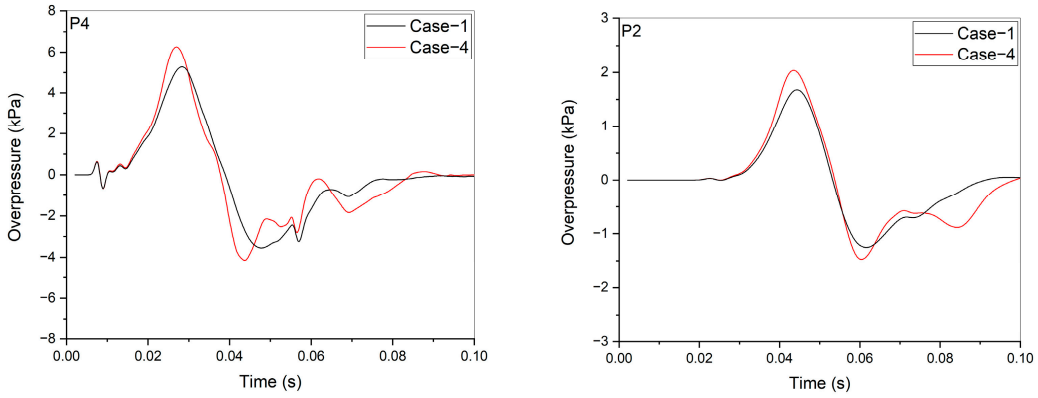

(**a**) (**b**)

Figure 9. Comparison of overpressures at local positions between Cases−1 and 4: (**a**) P4 (2 m front of the barrier); (**b**) P2 (2 m behind the barrier).

4. Producing Datasets Using Machine Learning

4.1. Development of the Neural Network Model

To develop a neural network model, using the open-source software of python 3.7 [37], TensorFlow 2.3.0 [38], and Keras 2.3.1 [39], capable of predicting the overpressures in the rear region of the barrier according to the barrier height and the distance from the explosion site during the VCE of the hydrogen–air mixture volume 5.2 m^3, we used the calculated overpressures for 0.1 s at the locations of P2, P6, and P7 with barrier heights of 2 m and 4 m (Figure 8) as the training data for the neural network model. This development of the neural network model started with a conceptual design model, as shown in Figure 10, which was configured with hidden layers, neurons, activation functions, and loss functions using the commercial software Mathematica [29,40,41]. The completed model consisted of eight hidden layers with different numbers of neurons and activation functions separately applied to each layer to minimize the loss value, as shown in Table 5. The loss value calculated by the mean squared error function in the developed neural network model was approximately ±1.24%.

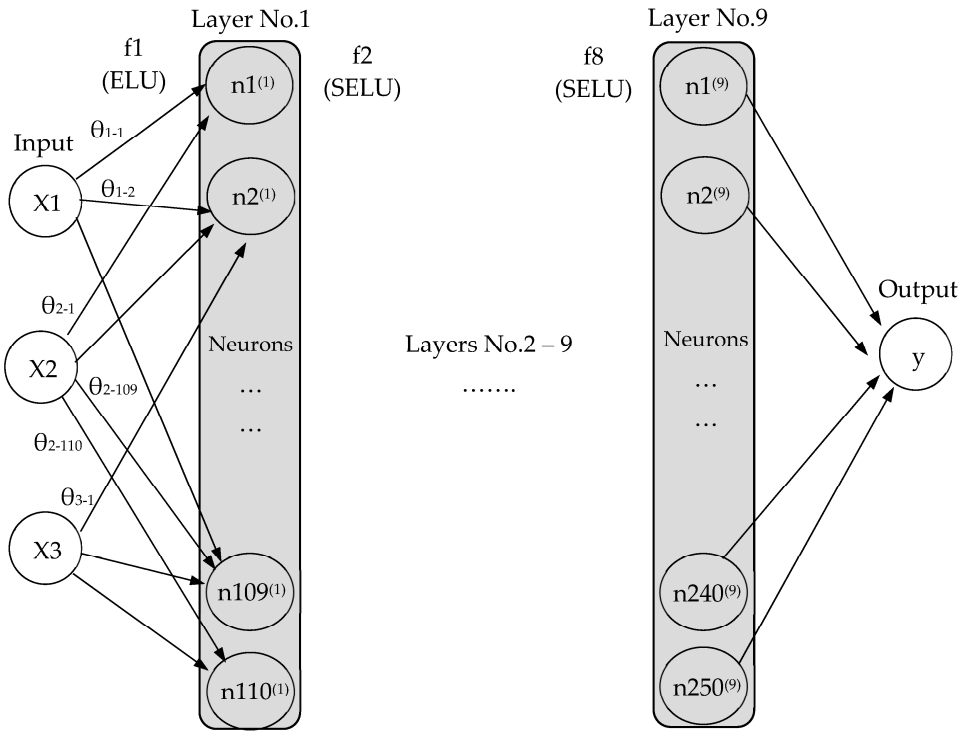

(**a**)

Function Name	Exponential Linear Unit (ELU)	Rectified Linear Unit (ReLU)	Self-Gated Activation Function (Swish)	Scaled Exponential Linear Unit (SELU)
Plot	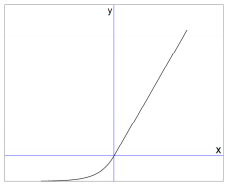	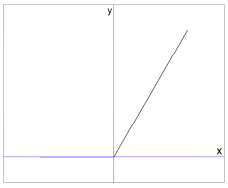	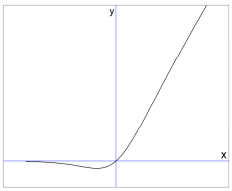	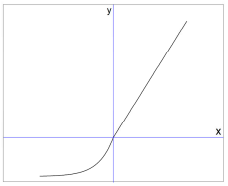
Numerical Expression	$\begin{cases} x \geq 0 & x \\ x < 0 & e^x - 1 \end{cases}$	$\begin{cases} x \geq 0 & x \\ x < 0 & 0 \end{cases}$	$\frac{x}{e^{\beta x}+1}, \quad \beta = -1$	$\begin{cases} x \geq 0 & 1.0507x \\ x < 0 & 1.7581(e^x - 1) \end{cases}$

(**b**)

Figure 10. Conceptual design of hidden layers, neurons, and activation functions for the neural network model: (**a**) Conceptual design model; (**b**) Plots and numerical expressions of the activation functions.

Table 5. Number of neurons and activation functions according to the hidden layers.

Hidden Layers	**Number of Neurons**	**Name of Activation Function**
1	110	Exponential Linear Unit (ELU)
2	280	Scaled Exponential Linear Unit (SELU)
3	190	Rectified Linear Unit (ReLU)
4	170	Exponential Linear Unit (ELU)
5	100	Self-Gated Activation Function (Swish)
6	140	Scaled Exponential Linear Unit (SELU)
7	50	Exponential Linear Unit (ELU)
8	70	Scaled Exponential Linear Unit (SELU)
9	250	Rectified Linear Unit (ReLU)

Loss Function and Value: Mean Squared Error and 0.0124; Learning Rate: 0.0005.

4.2. Overpressure Data Produced by the ML Method and Discussion

The overpressure data produced at the P2, P6, and P7 locations by the developed neural network model for barrier heights of 2.5 m and 3.5 m during VCE with a hydrogen–air mixture volume of 5.2 m^3 are shown in Figure 11. From a comparison of the overpressures between the data produced by the ML method and the training data for the neural network model, we can judge that the data generated by the ML method accurately represent the characteristics of the pressure wave in the rear region of the barrier. The peak overpressures at P2, P6, and P7 locations decrease as the barrier height increases and the distance from the ignition point increases.

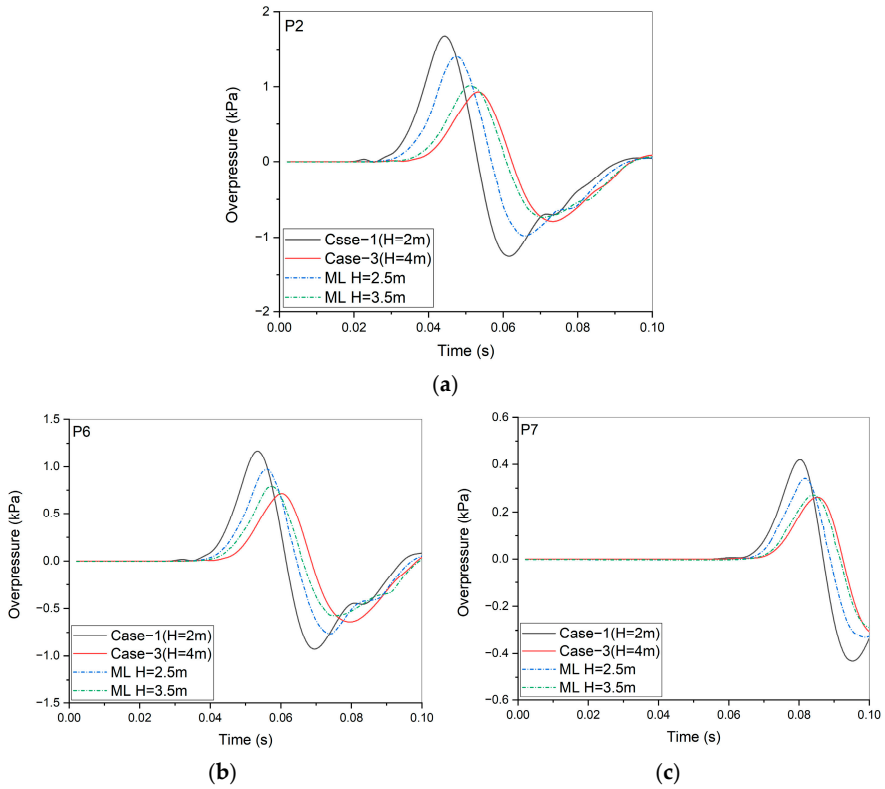

Figure 11. Overpressure data produced in the rear region of the barrier using the ML method: (**a**) P2 (2 m behind the barrier); (**b**) P6 (range: 11 m); (**c**) P7 (range: 21 m).

Therefore, we can expect that the ML method will be effective when used to extend the datasets using credible data in a VCE database when proper datasets for safety evaluations of HRSs to be constructed around protected facilities do not exist. However, through this study, which generated overpressures using the ML method, we also found that a neural network model that considers the features of pressure wave propagation, which arose in the area in front of the barrier and the region behind the barrier, should be developed separately.

5. Conclusions

A methodology was developed to configure a database to provide criteria to safety engineers who will conduct CFD analyses of hypothetical VCE accidents to evaluate the safety of HRSs to be constructed around protected facilities in a large city. The proposed methodology is to extend the datasets in the VCE database using the CFD sensitivity calculations and the ML method on the basis of measured data obtained from VCE experimentation, assuming the installation of a barrier wall. CFD sensitivity calculations using an established analysis methodology for the VCE phenomena will not only generate new datasets but will also provide visualized results to support evaluations by safety engineers. In addition, datasets based on various grid models in CFD sensitivity calculations can

provide a guideline for the development of a grid model for VCE accident analyses in HRSs. We also uncovered the possibility of using the ML method to produce new datasets quickly when proper test datasets for comparisons with CFD analysis results for hypothetical VCE accidents do not exist. However, from this study, we realized that the training dataset to be used should be carefully chosen, considering the application purpose when developing a neural network model. Finally, we conclude such an extended VCE database, as discussed here, can sufficiently compensate for the lack of gas explosion test results with a barrier installed and can be effectively used as a reference tool to increase the safety of HRSs in Republic of Korea.

6. Future Studies

The datasets produced by the CFD sensitivity calculation and the ML method will be examined to confirm their validity and applicability after related test data are produced experimentally. VCE accident simulations with the installation of various barrier models in HRSs will be conducted, and their results will be confirmed on the basis of the datasets in the VCE database.

Author Contributions: Conceptualization, C.-H.Y.; methodology, H.-S.K. and J.-W.H.; software, H.-S.K. and J.-W.H.; validation, H.-S.K. and J.-W.H.; formal analysis, H.-S.K. and J.-W.H.; investigation, H.-S.K. and C.-H.Y.; resources, H.-S.K. and J.-W.H.; data curation, H.-S.K. and J.-W.H.; writing—original draft preparation, H.-S.K.; writing—review and editing, J.-W.H. and H.-S.K.; visualization, H.-S.K.; supervision, H.-S.K.; project administration, C.-H.Y.; funding acquisition, C.-H.Y. All authors have read and agreed to the published version of the manuscript.

Funding: This work was supported by a grant from the Korea Institute of Energy Technology Evaluation and Planning (KETEP) funded by the Korean government (Ministry of Trade, Industry and Energy) (No. 20215810100020).

Data Availability Statement: Research data will be provided through the official website that will be operated by KGS and Dahan Tech Inc. after the completion of the research project.

Conflicts of Interest: The authors declare no conflict of interest.

Nomenclature

Variable	Definition	Unit
a_{wv}	Absorption coefficient of water vapor	[−]
E	emission contribution	[−]
ft	Fuel mixture fraction	[−]
G	radiation intensity	[W/m^2]
h	Enthalpy	[J/kg]
K	Thermal conductivity	[W/m·K]
k	Absorption coefficient depending on the gas temp.	[−]
p	Pressure	[Pa]
q	Heat flux	[W/m^2]
S_i	Source/Sink of species-i	[kg/m^2·s]
S_u	Laminar flame speed	[m/s]
S_{ct}	Turbulent Schmidt number	[−]
T	Temperature	[K]
U	Velocity	[m/s]
Y_i	Species-i mass fraction	[−]
μ_t	Turbulence effective viscosity	[kg/m·s]
ρ	Density	[kg/m^3]
σ_{SB}	Stefan-Boltzmann coefficient	[−]
φ	Fuel equivalent ratio	[−]
Subscripts		
o	Reference condition	
u	Unburned	
wv	Water vapor	

References

1. Ministry of Trade, Industry, and Energy. *Hydrogen Economy Fostering and Hydrogen Safety Management Act*; No. 16942; Ministry of Trade, Industry, and Energy: Sejong, Republic of Korea, 2021.
2. National Library of Korea. Hydrogen Economy Revitalization Roadmap, Policy Information. 2019. Available online: https://policy.ni.go.kr (accessed on 23 September 2023).
3. Chuncheon District Prosecutors' Office, Gangneung Branch. *Investigation Results for the Hydrogen Tank Explosion in Gangwon Techno Park*; Press Release Report; Chuncheon District Prosecutors' Office, Gangneung Branch: Gangneung, Republic of Korea, 2019.
4. International Atomic Energy Agency. *The Fukushiama Daiichi Accident, Vol. 1, Description and Context of the Accident*; Technical Report; International Atomic Energy Agency: Vienna, Austria, 2015.
5. International Atomic Energy Agency. *IAEA Review of Safety Related Aspects of Handling ALPS Treated Water at TEPCO's Fukushima Daiichi Nuclear Power Station*; Technical Report; International Atomic Energy Agency: Vienna, Austria, 2023.
6. Yoon, B.H. Hydrogen refueling station deployment can't keep up with hydrogen vehicles. In *Electronic Times*; Korea Electricity Newpaper: Seoul, Republic of Korea, 2023.
7. Kang, S.G.; Kim, H. Liquid hydrogen technology trends and safety standards development status. In Proceedings of the Korean Institute of GAS Spring Meeting, Jeju, Republic of Korea, 26–27 May 2022.
8. Kim, K.S. *Development of Design Technology and Safety Standard in the Protection Wall for Blast Mitigations in a Hydrogen Station*; Research Plan Report, No. 20215810100020; Korea Gas Safety Corporation: Yeongwol, Republic of Korea, 2021.
9. *KGS FP216*; Facility/Technical/Inspection Code for Fuel Vehicles Refueling by Type of On-Site Hydrogen Production. Korea Gas Safety Corporation: Eumseong, Republic of Korea, 2020.
10. *KGS FP217*; Facility/Technical/Inspection Code for Fuel Vehicles Refueling by Type of Compressed Hydrogen Delivery. Korea Gas Safety Corporation: Eumseong, Republic of Korea, 2020.
11. You, E.G.; Kim, M.I.; Lee, Y.S.; Kang, S.G. A study in the risk assessment of LH2 refueling station. In Proceedings of the Korean Institute of GAS Spring Meeting, Jeju, Republic of Korea, 25–26 May 2023.
12. Kwon, D.; Choi, S.K.; Yu, C. Improved Safety by Crossanalyzing quantitative risk assessment of hydrogen refueling stations. *Int. J. Hydrogen Energy* **2022**, *47*, 10788–10798. [CrossRef]
13. Li, Z.; Pan, X.; Meng, X.; Ma, J. Study on the harm effects of releases from liquid hydrogen tank by consequence modeling. *Int. J. Hydrogen Energy* **2012**, *37*, 10624–17629. [CrossRef]
14. *KOSHA P-31-2001*; Predictive Methods for Accident Damage. Korea Occupational Safety and Health Agency: Ulsan, Republic of Korea, 2001.
15. Sochet, I.; Viossat, A.-L.; Rouyer, J.-L.; Hemmerich, P. Safe hydrogen generation by nuclear HTR. In Proceedings of the ICAPP-2004, Pittsburg, PA, USA, 13–17 June 2004.
16. Kang, H.S.; NO, H.C.; Kim, S.B. Application of the developed CFD analysis methodology to H_2 explosion accidents in an open space. *Int. J. Hydrogen Energy* **2017**, *42*, 1306–1317. [CrossRef]
17. Shen, R.; Jiao, Z.; Parker, T.; Sun, Y.; Wang, Q. Recent application of computational fluid dynamics (CFD) in process safety and loss prevention: A review. *J. Loss Prev. Process Ind.* **2020**, *67*, 104252. [CrossRef]
18. Kim, S.M.; Kang, H.S.; Choi, K.S. *radXiFoam v1.0*; VCE Solver; KAERI: Daejeon, Republic of Korea. Available online: https://github.com/ksm0226/radXiFoam (accessed on 23 September 2023).
19. OpenCFD Ltd. *OpenFOAM-v2112 User Guide*; Technical Report; ESI: Rungis, France, 2021. Available online: https://www.openfoam.com (accessed on 23 September 2023).
20. Kang, H.S.; No, H.C.; Kim, S.B.; Kim, M.H. Methodology of CFD analysis for evaluating H_2 explosion accidents in an open space. *Int. J. Hydrogen Energy* **2015**, *40*, 3075–3090. [CrossRef]
21. Wen, J.X.; Marnon, M.; Moretto, P.; Reinceke, E.-A.; Sathiah, P.; Studer, E.; Vyazmina, E.; Melideo, D. Statistics, lessons learned and recommendations from analysis of HIAD 2.0 database. *Int. J. Hydrogen Energy* **2022**, *47*, 3075–3090. [CrossRef]
22. ARIA. Available online: https://www.aria.developpement-durable.gouv.fr (accessed on 23 September 2023).
23. RISCAD. Available online: https://riss.aist.go.jp/sanpo/riscad (accessed on 23 September 2023).
24. Groethe, M.A.; Colton, J.D. *FY01 Annual Report on Hydrogen Safety in the World Energy Network*; Technical Report; SRI: Menlo Park, CA, USA, 2002.
25. Groethe, M.A. *FY02 Annual Report on Hydrogen Safety in the World Energy Network*; Technical Report; SRI: Menlo Park, CA, USA, 2002.
26. Bangert, P. *Machine Learning and Data Science in the Power Generation Industry*, 1st ed.; Elsevier: Amsterdam, The Netherlands, 2021.
27. Krishnan, S.; Yang, Z.; Hellerstein, J.; Stoica, I. What Is the Role of Machine Learning in Database? Available online: https://rise.cs.berkeley.edu/blog (accessed on 23 September 2023).
28. Nozu, T.; Tanaka, R.; Ogawa, T.; Hibi, K.; Sakai, Y. Numerical simulation of hydrogen explosion tests with a barrier wall for blast mitigation. In Proceedings of the ICHS-2005, Pisa, Italy, 8–10 September 2005.
29. Hwang, J.; Park, S.; Lee, Y.; Min, H. Research on predicting liquid-hydrogen explosion pressure using machine learning. In Proceedings of the Korean Institute of GAS Spring Meeting, Jeju, Republic of Korea, 26–27 May 2022.
30. Choi, J.Y.; Jeung, I.S.; Yoon, Y. Computational fluid dynamics algorithms for unsteady shock-induced combustion, part 1: Validation. *AIAA J.* **2000**, *38*, 1179–1187. [CrossRef]

31. Mossi, A.; Galarca, M.M.; Brittes, R.; Vielmo, H.A.; Franca, F.H.R. Comparison of spectral models in the computation of radiative heat transfer in participating media composed of gases and soot. *ABCM J.* **2012**, *34*, 112–119. [CrossRef]
32. Modest, M.F. *Radiative Heat Transfer, International Editions*; McGraw-Hill, Inc.: Singapore, 1993.
33. Kim, S.; Kim, J. Effect of radiation model on simulation of water vapor—Hydrogen premixed flame using flamelet combustion model in OpenFOAM. *Nuclear Eng. Tech.* **2022**, *54*, 1321–1335. [CrossRef]
34. Metghalchi, M.; Keck, J.C. Burning velocities of mixtures of air with methanol, isooctane, and indolence at high pressure and temperature. *Combust. Flame* **1982**, *48*, 191–210. [CrossRef]
35. Koroll, G.W.; Kumar, R.K.; Bowles, E.M. Burning velocities of hydrogen-air mixtures. *Combust. Flame* **1993**, *94*, 330–340. [CrossRef]
36. Kang, H.-S.; Kim, S.-M.; Kim, J. Safety issues of a hydrogen refueling station and a prediction for an overpressure reduction by a barrier using OpenFOAM software for an SRI explosion test in an open space. *Energies* **2022**, *15*, 7556. [CrossRef]
37. Python 3.7.0. Available online: https://python.org (accessed on 23 September 2023).
38. TensorFlow 2.3.0. Available online: https://www.tensorflow.org (accessed on 23 September 2023).
39. Keras 2.3.1. Available online: https://pypi.org/project/keras (accessed on 23 September 2023).
40. Wolfram. Neural Networks. Available online: https://reference.wolf.com/language/guide/NeuralNetworks.html (accessed on 23 September 2023).
41. Cho, J. Risk Assessment for a Severe Accident Using a Deep Learning Technology. In Proceedings of the KAERI, Daejeon, Republic of Korea, 13 December 2021.